

## Couple stress nanofluid flow through a bifurcated artery — Application of catheterization process

KM Surabhi<sup>1</sup>      Arpitha Ravikanti<sup>1</sup>  
D. Srikanth<sup>1,\*</sup>      D. Srinivasacharya<sup>2</sup>

**Abstract.** In this article, we are exploring the hemodynamics of nanofluid, flowing through a bifurcated artery with atherosclerosis in the presence of a catheter. For treating obstruction in the artery, one can use the catheter whose outer surface is carrying the drug coated with nano-particles. The resultant solvent is considered as blood nano-fluid. Blood being a complex fluid, is modeled by couple stress fluid. In the presence of nano-particles, the temperature and the concentration distribution are understood in a bifurcated stenotic artery. The concluded mathematical model is governed by coupled non-linear equations, and are solved by using the homotopy perturbation method. Consequently, we have explored is the effects of fluid and the embedded geometric parameters on the hemodynamics characteristics. It is also realized that high wall shear stress exists for couple stress nano-fluid when compared to Newtonian nano-fluid. which is computed at a location corresponding to maximum constriction ( $z = 12.5$ ) of the artery.

### §1 Introduction

World Health Organization (WHO) recognizes that the disorders in the cardiovascular system are leading to morbidity and mortality globally. According to the organizations report [1], Non-communicable Diseases (NCDs) are responsible for premature deaths, out of which, one third are occurring due to Cardiovascular Diseases (CVDs). These generally designate the conditions in which, the patients have narrowed or thickened blood vessels, medically termed as stenosis, which can lead to heart attack, angina (chest pain) or stroke.

Blood is a complex living fluid, which nurtures life and includes a variety of cells like leukocytes, erythrocytes, and platelets. It is to be noted that the erythrocytes are responsible for the transport of oxygen,  $CO_2$ , and other nutrients to the different organs of the human body, as discussed by Fung [2]. Several researchers understood blood rheology [3, 4, 5] for the Newtonian fluid. Bugliarello et al. [6] macroscopically observed the suspension of the

---

Received: 2019-10-08.      Revised: 2020-04-16.

MR Subject Classification: 35Q35, 35Q30, 76A05, 76Z05.

Keywords: couple stress fluid, bifurcated stenotic artery, homotopy perturbation method, wall shear stress.

Digital Object Identifier(DOI): <https://doi.org/10.1007/s11766-021-3924-1>.

Supported by Council of Scientific and Industrial Research (CSIR), INDIA (25(0262)/17/EMR-II).

\*Corresponding author.

neutrally buoyant cells in the blood, which undergo deformation. These deformations are demonstrated in the form of constitutive expressions of viscosity and shear stress. Some such fluids are listed under the non-Newtonian category. In such fluids, the corpuscles radius of gyration is different from that of fluid particles. This difference produces couple stresses in the fluid, along with the deformation of the particles. The fluid which has the above two attributes is called a couple stress fluid and is demonstrated by Stokes [7]. The study of blood flow with couple stresses may play a significant part in interpreting the rheological anomalies associated with the blood flow. [8] has shown A detailed hemodynamics in the aorta from the medical imaging data. Chakravarty [9] considered the blood as a classical viscous fluid and analyzed the flow characteristics by incorporating the numerical methods in a bifurcated aorta. Cardiac catheterization is an invasive surgical technique developed by Werner Forssmann after practically testing it on himself. The same has been discussed in detail by Truss et al.[10]. In the exhibits of their investigation as done by various researchers [11, 12, 13, 14, 15], the mathematical model was constructed by accounting for the rigidity of the arterial wall and the flow dynamics were studied for mild stenosis, by considering the blood as couple stress fluid.

In the advanced pharmaceutical and therapeutic techniques for the diagnosis and treatment of the CVDs, effective usage of the nanotechnology concepts is prime. Nano-Medicine is the phenomena of using nanotechnology for the delivery of the drug at a specified location in a quick time. This medication technique, bearing the ultimate objective of a controlled and sustainable release of drug at the site of infection in human organs, enhances the therapeutic activity of drug while minimizing the side effects. [16, 17, 18, 19] understood the dynamics of nanofluid in the stenotic artery using the numerical schemes under Newtonian structure. An intense research work done on nanofluid to enrich its importance in various application, can be understood from the articles [20, 21, 22, 23, 24].

Various numerical, optimization and perturbation techniques are in use to solve the complex fluid flow problems. With this view, researchers [25, 26, 27] used various techniques to solve the non-linear equations in various domains. However, these asymptotic methods have their limitations. Mostly, all perturbation techniques depend on the assumption of a small parameter which exists in the modeled equations. This consideration of small parameter automatically imposes some restrictions on the solution technique, and therefore, the solution is obtained. Determination of such a small parameter for all non-linear problems is non-trivial and in some cases may not be possible at all. To overcome the need of small parameters, some solution techniques are introduced such as Artificial parameter method by Liu [28], Homotopy analysis method by Liao [29], Variational iteration method by JH He [30]. Later, JH He [31] presented a technique which took care of all the importance of Homotopy analytical method as well as the traditional perturbation method and is named as homotopy perturbation method (HPM). In this methodology, one constructs the homotopy involving an embedding parameter  $q$ , for the variables to be computed. These to be computed variables are then expressed in the series form of various powers of  $q$ . The embedding parameters account for the values from  $[0, 1]$ . Some of the researchers [32, 33] utilized this method for solving the mathematical model of stenotic arteries to understand the hemodynamics.

In this paper, we analyzed the physiological flow dynamics of nanofluid flow through a bifurcated stenotic artery under the influence of a catheter. The mathematical model governed by coupled non-linear equations is solved by using the HPM. We analyzed the effects of fluid

and embedded geometric parameter on the hemodynamics characteristics of blood, such as pressure drop, flow resistance, and wall shear stress (WSS). Also, a comparison of the results of wall shear stress and impedance of the flow to the results of Newtonian nanofluid is done. As far as the organization of the paper goes, Sect. 2 discusses the mathematical modeling of the proposed model. Sect. 2.2 demonstrates the method and its implementation procedures, and Sect. 2.2 discusses the obtained outcomes, while sections 2.2 and 2.2 contains the conclusions and acknowledge respectively.

## §2 Mathematical Modeling Assumptions and Justifications

### 2.1 Description of the flow geometry

Consider a laminar, incompressible non-Newtonian nano-fluid flowing through a bifurcated stenotic artery in the presence of a catheter, as depicted in Fig. 1. The mathematical model of the proposed work is subject to certain assumptions as given below,

1. Bifurcation of artery is assumed to be symmetrical in nature and bifurcated daughter arteries are straight circular cylinders of finite length.
2. Parent artery is endowed with the symmetrical mild stenosis in its lumen.
3. For treating the obstruction in the parent artery, catheterization procedure is adopted in the axial direction, whose outer surface is layered with the temperature-sensitive drug, coated with NPs.
4. Couple stress fluid is considered for the computation, which theoretically mimicks the behavior of blood.
5. In the bifurcated artery of the aorta, curvature is at apex of the artery, as shown in Fig. 1.

Mathematical expressions of a bifurcated stenotic artery with inner and outer wall are taken from [9], and these equations given as (1) and (2). Outer wall of the geometry is given as:

$$R_1(z) = \begin{cases} a; & 0 \leq z \leq d \text{ and } d + L_0 \leq z \leq z_1 \\ [a - \frac{4\epsilon}{L_0^2} (L_0(z-d) - (z-d)^2)]; & d \leq z \leq L_0 + d \\ [a + r_0 - \sqrt{r_0^2 - (z - z_1)^2}]; & z_1 \leq z \leq z_2 \\ [2r_1 \sec \beta + (z - z_2) \tan \beta]; & z_2 \leq z \leq z_{max} \end{cases} \quad (1)$$

Inner wall of artery is expressed as:

$$R_2(z) = \begin{cases} 0; & 0 \leq z \leq z_3 \\ [\sqrt{r_0'^2 - (z - z_3 - r_0')^2}]; & z_3 \leq z \leq z_3 + r_0' (1 - \sin \beta) \\ [r_0' \cos \beta + z_4]; & z_3 + r_0' (1 - \sin \beta) \leq z \leq z_{max} \end{cases} \quad (2)$$

Here,  $R_1(z)$  and  $R_2(z)$  are the radii of outer wall and inner wall of the bifurcated stenotic artery respectively. Radius of parent artery is represented by  $a$ , which is having a mild stenosis of the length  $L_0$  at a distance  $d$  from the origin. In bifurcated artery,  $r_1$  corresponds to the radius of daughter artery, while  $r_0$  and  $r_0'$  correspond to the radii of curvatures for lateral junction and flow divider respectively while  $r_c$ , represents the radius of a catheter placed along the flow direction. In the process of the bifurcation of the parent artery,  $z_1$  and  $z_2$  are recorded as the

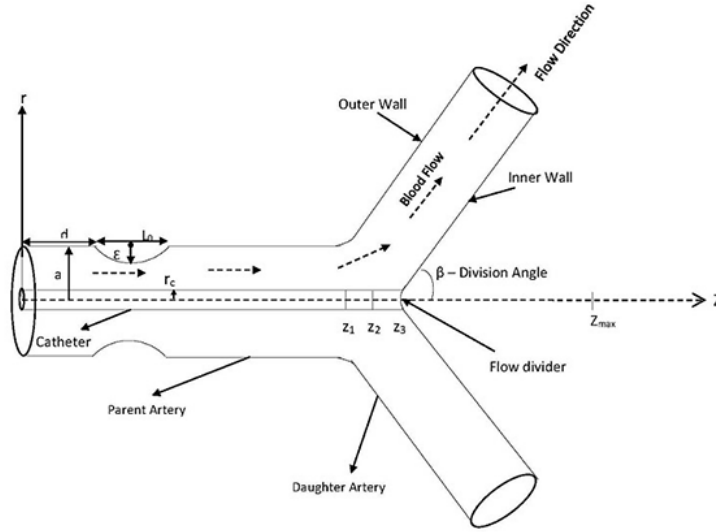


Figure 1. Pictorial representation of a bifurcated stenotic artery.

onset and offset locations of the lateral junction, while  $z_3$  is at the apex with the bifurcation angle being  $\beta$ . Also  $\epsilon$  represents the maximum height of the stenosis at the point  $z = d + L_0/2$ . For convenient simulation of the physiological parameters, fluid domain is considered to be of finite length and accordingly the length of the bifurcated stenotic artery is represented by  $z_{max}$ . Expression of the parameters which are accommodated in the flow geometry represented by Fig. 1, are mathematically expressed as:

$$z_2 = z_1 + (a - 2r_1 \sec \beta) \frac{\sin \beta}{(\cos \beta - 1)}$$

$$z_3 = z_2 + q$$

where, the value of  $q$  is chosen to be sufficiently small lying in the interval  $(0.1, 0.4)$  validating the requirements of geometry.

$$z_4 = \left[ z - z_3 - r'_0 (1 - \sin \beta) \right] \tan \beta$$

$$r_0 = \frac{(a - 2r_1 \sec \beta)}{(\cos \beta - 1)}$$

$$r'_0 = \frac{(z_3 - z_2 \sin \beta)}{(1 - \sin \beta)}$$

## 2.2 Thermo-physical properties of nanofluid

Fahraeus et al.[34] investigated the influence of diameter of capillaries tubes on the viscosity of the blood, which is a consequence of deformability of erythrocytes in the plasma. Viscosity is a vital characteristic of the blood which facilitates the fluid flow through the arteries. During the process of fluid flow through the cylinder, the flow is more effective at the main flow region than at the boundary of the cylinder. In this situation, the velocity profile takes the parabolic shape. The immersion of nano-particels (NPs) in the flow domain leads to the variation in the

viscosity of the corresponding fluid, which is interesting to study.

Batchelor [35] developed the formula for viscosity in 1972 for high volume fraction approximate ( $\Phi \leq 4\%$ ) by considering the Brownian motion effect. The mathematical relation corresponding to viscosity in this case is written as,

$$\mu_{nf} = \mu_f(1 + 2.5 \Phi + 6.5 \Phi^2). \tag{3}$$

In these articles, authors intended to present the influence of NPs on base fluid properties by considering *Ag*- NPs, *Cu*- NPs, *Al<sub>2</sub>O<sub>3</sub>*- NPs and *TiO<sub>2</sub>*- NPs. Their corresponding empiric relations justified with the experiments, are reported in the form of table 1.

Table 1. Thermo-physical properties of nano-fluids.

	<i>H<sub>2</sub>O</i>	Blood obtained from [33]	<i>Al<sub>2</sub>O<sub>3</sub></i>	<i>Ag</i>	<i>Cu</i>	<i>TiO<sub>2</sub></i>
$C_p(J/kgK)$	4179	3617	765	235	385	686.2
$\rho(kg/m^3)$	1000	1060	3970	10500	8933	4250
$k(W/mK)$	0.613	0.52	40	429	401	8.9538
$\gamma \times 10^{-5}(K^{-1})$	21	-	0.85	1.89	1.67	1.9
$\mu_{nf}/\mu_f$	1	-	$1 + 39.11\Phi + 533.9\Phi^2$ , as given by [36]	$1.005 + 0.497\Phi - 0.1149\Phi^2$ as given by Godson et al. [38]	$\frac{1}{(1-\Phi)^{2.5}}$ as given by Brinkman [39]	$1 + 5.45\Phi + 108.2\Phi^2$ as given by Bock Choon & Young Cho [37]
$\eta_{nf}/\eta_f$	1	-	$1 - 39.11\Phi - 533.9\Phi^2$	$1.005 - 0.497\Phi + 0.1149\Phi^2$	$\frac{1}{(1+\Phi)^{2.5}}$	$1 - 5.45\Phi - 108.2\Phi^2$
$k_{nf}/k_f$	1	-	$1 + 7.47\Phi$ as given by Bock Choon & Young Cho [37]	$0.9508 + 0.9692\Phi$ as given by Godson et al.[38]	$\left( \frac{k_{np} + (n - 1)k_f + (n - 1)\Phi(k_{np} - k_f)}{(k_{np} + (n - 1)k_f + \Phi(k_f - k_{np}))} \right)$ as given by Hamilton [40]	$1 + 2.92\Phi - 11.99\Phi^2$ as given by Bock Choon & Young Cho [37]

The empiric relation in case of effective nano-fluid for thermo-physical properties follow the convective phenomena of nano-fluids as discussed by Buongiorno et al.[41]. These specific relations of nano-fluid are given as,

$$\rho_{nf} = (1 - \Phi)\rho_f + \Phi\rho_p \tag{4}$$

$$(\rho c_p)_{nf} = (1 - \Phi)(\rho c_p)_f + \Phi(\rho c_p)_p \tag{5}$$

$$(\rho \gamma)_{nf} = (1 - \Phi)(\rho \gamma)_f + \Phi(\rho \gamma)_p. \tag{6}$$

### 2.3 Equations governing the flow

Consider an axisymmetric, incompressible, nano-fluid flow in a non-uniform region, as depicted in figure 1. Nano-fluid is a composition of two components under the following assumptions,

1. Flow driven by a constant pressure gradient.
2. Negligible radiative heat transfer.
3. No chemical reaction between the fluid and NPs.
4. Thermal equilibrium exists between the base fluid and NPs.

Equations governing the flow are obtained from [33] given under,

$$\nabla \cdot \vec{V} = 0 \tag{7}$$

$$\rho_{nf} (\partial_t \vec{V} + \vec{V} \cdot \nabla \vec{V}) = -\nabla p + \mu_{nf} \nabla^2 (\vec{V}) - \eta_{nf} \nabla^4 (\vec{V}) + F \tag{8}$$

$$\partial_t T + (\vec{V} \cdot \nabla) T = \frac{\kappa_{nf}}{(\rho c_p)_{nf}} \nabla^2 T + \frac{(\rho c_f)_{nf}}{(\rho c_p)_{nf}} \left[ D_B \nabla C \cdot \nabla T + \frac{D_T}{T_1} \nabla T \cdot \nabla T \right] \tag{9}$$

$$\partial_t C + (\vec{V} \cdot \nabla) C = D_B \nabla^2 C + \left( \frac{D_T}{T_1} \right) \nabla^2 T \tag{10}$$

Here, velocity vector is defined as  $\vec{V} = (u(r, z), 0, v(r, z))$  and  $F$  is the body force. It is to be noted that the body force  $F$  experienced by the fluid is due to the variation in the density, and this density variation is addressed by the use of Boussinesq approximation in the momentum equation.  $T$  and  $C$  represent the temperature and concentration of blood-nano fluid while  $T_1$  is the ambient temperature of fluid. Here, for the resultant nano-fluid,  $\mu_{nf}$  and  $\eta_{nf}$  are the dynamic viscosity and couple stress viscosity respectively.  $\kappa_{nf}$  corresponds to the thermal conductivity,  $(\rho c_p)_{nf}$  and  $(\rho c_f)_{nf}$  adhere to the specific heat capacitance of the nano-particles and heat capacitance of nano-fluid respectively. Brownian diffusion coefficient and thermophoresis diffusion coefficients are accorded by  $D_B$  and  $D_T$  respectively.

### 2.4 Non-dimensionalization of the governing equations

Non-dimensionalization is a powerful tool in fluid mechanics, which enables us to obtain a great deal of insight. In this problem, the dimensionless variables that are introduced are given by

$$\begin{aligned} r' &= r/a, \quad z' = z/L_0, \quad d' = d/L_0, \quad R'_1(z') = R_1(z)/a, \\ R'_2(z') &= R_2(z)/a, \quad t' = t u_0/L_0, \quad v' = v/u_0, \\ \theta &= (T - T_0)/(T_1 - T_0), \quad \sigma = (C - C_0)/(C_1 - C_0), \\ u' &= u L_0/(u_0 \epsilon), \quad p' = p a^2/(u_0 L_0 \mu_f) \end{aligned} \tag{11}$$

where,  $a$  denotes the characteristic length of the artery and  $u_0$  is characteristic flow velocity in the flow regime. Non-dimensionalised form of the governing equations (7)-(10) after incorporating the non-dimensional variables from equation (11), subject to the conditions of the mild stenosis of the geometry, represented by  $\xi(= \epsilon/a) \ll 0$  and  $\delta(= a/L_0) \approx O(1)$ , are given by

$$\partial_z v = 0 \quad (12)$$

$$\partial_r p = 0 \quad (13)$$

$$\partial_z p = \frac{\mu_{nf}}{\mu_f} \left( \partial_{rr} v + 1/r \partial_r v \right) - \frac{\eta_{nf}}{\eta_f} \frac{1}{\beta^2} \left[ \partial_{rrrr} v + 2/r \partial_{rrr} v - 1/r^2 \partial_{rr} v + 1/r^3 \partial_r v \right] + \frac{(\rho\gamma)_{nf}}{(\rho\gamma)_f} (\theta Gr + \sigma Br) \quad (14)$$

$$\partial_{rr} \theta + 1/r \partial_r \theta + N_b (\partial_r \sigma \partial_r \theta) + N_t (\partial_r \theta)^2 = 0 \quad (15)$$

$$\partial_{rr} \sigma + 1/r \partial_r \sigma + N_t/N_b (\partial_{rr} \theta + 1/r \partial_r \theta) = 0 \quad (16)$$

Non-dimensionalization process recovers some characteristic non-dimensional numbers which are analysed appropriately. Accordingly we obtained  $Gr = \frac{a^2 (\rho\gamma)_f (T_1 - T_0)}{u_0 \mu_f}$ , the Grashof number and  $Br = \frac{a^2 (\rho\gamma)_f (C_1 - C_0)}{u_0 \mu_f}$ , the solute Grashof number. Brownian motion parameter is  $N_b = \frac{\tau_{nf} D_B (C_1 - C_0)}{\alpha_{nf}}$  and thermophoresis parameter is  $N_t = \frac{\tau_{nf} D_T (T_1 - T_0)}{\alpha_{nf} T_1}$ . Further,  $\beta^2 = (\eta_f a^2)/\mu_f$  is length dependent parameter.

## 2.5 Non-Dimensional boundary conditions

Treatment and diagnosis of diseases related to atherosclerosis are different. Therefore, rheological properties and the flow behavior of blood is of immense importance for fundamental understanding. Considering this point of view, Chaturani [42] stated different kinds of boundary conditions for polar fluids.

Hyper-stick condition, considered at a catheter wall is as given below,

$$v = 0 \text{ at } r = r_c \text{ where } 0 \leq z \leq z_3 \quad (17)$$

Further, Brunn [43] introduced the importance of slip velocity at the wall for the different flow domains, for the polar fluids. Attributing this theory, slip velocity is considered, at the arterial wall to a bifurcated artery. For outer artery wall ,

$$v = u_2 \text{ at } r = R_1(z) \text{ where } d \leq z \leq d + L_0 \quad (18)$$

$$v = u_1 \text{ at } r = R_1(z) \text{ where } 0 \leq z \leq d \quad (19)$$

$$\text{and } d + L_0 \leq z \leq z_{max}$$

$$v = u_3 \text{ at } r = R_1(z) \text{ where } z_3 \leq z \leq z_{max} \quad (20)$$

For inner artery wall,

$$v = 0 \text{ at } r = R_2(z) \text{ where } z_3 \leq z \leq z_{max} \quad (21)$$

Where  $u_1$ ,  $u_2$  and  $u_3$  are constant slip velocity with which the blood flows between the outer and inner arterial wall respectively.

Boundary conditions for dimensionless temperature and concentration are given below as,

$$\theta = 1, \sigma = 1, \text{ at } r = r_c \quad (22)$$

$$\theta = 0, \sigma = 0, \text{ at } r = R_1(z) \text{ and } r = R_2(z) \forall z \quad (23)$$

We are seeking such kind of boundary conditions for temperature and concentration variables, due to the insertion of a catheter coated with the temperature-sensitive drug into the blood beds. Therefore, high temperature is noted on the surface of a catheter. This enhancement in the temperature helps to release the drug faster in the flow regime. This consideration reveals that the temperature sensitive drug coated catheter is inserted into the lumen of the artery, which shows that the drug is highly concentrated at the catheter surface. Further, it is to be noted that an external temperature is provided on the surface of the catheter for the release of the drug.

### §3 Solution methodology

In order to accomplish the solution of the non-linear coupled governing equations, HPM method proposed by JH He [31], which is the combination of homotopy and traditional perturbation methods, is considered. This overcomes the limitations of traditional perturbation methods. Here an embedding parameter  $q$  belonging to the interval  $[0, 1]$  is considered and the solutions are obtained by solving the system of equations which are obtained by comparing various powers of  $q$ . Here the initial solution is obtained conveniently by using the linear part of the non linear differential equation. Further, this technique has the full advantage of traditional perturbation techniques.

#### 3.1 Implementation of HPM to the present model

The coupled non-linear equations of temperature and concentration (15) and (16) respectively, are solved by applying HPM. We followed the same steps as implemented in the report [32]. From the equations (15) and (16), corresponding linear operator ( $L$ ) and non-linear operator ( $N$ ) are given below as,

$$\underbrace{\partial_{rr}\theta + 1/r \partial_r\theta}_L + \underbrace{N_b \partial_r\sigma \partial_r\theta + N_t (\partial_r\theta)^2}_N = 0 \tag{24}$$

$$\underbrace{\partial_{rr}\sigma + 1/r \partial_r\sigma}_L + \underbrace{N_t/N_b (\partial_{rr}\theta + 1/r \partial_r\theta)}_N = 0 \tag{25}$$

The required homotopy is constructed as,

$$H(\theta_h, q) = \partial_{rr}\theta_h + 1/r\partial_r\theta_h - (\partial_{rr}\theta_0 + 1/r\partial_r\theta_0) + q(\partial_{rr}\theta_0 + 1/r\partial_r\theta_0) + q[N_b\partial_r\sigma_h \partial_r\theta_h + N_t (\partial_r\theta_h)^2] = 0 \tag{26}$$

$$H(\sigma_h, q) = \partial_{rr}\sigma_h + 1/r\partial_r\sigma_h - (\partial_{rr}\sigma_0 + 1/r\partial_r\sigma_0) + q(\partial_{rr}\sigma_0 + 1/r\partial_r\sigma_0) + q[N_t/N_b(\partial_{rr}\theta_h + 1/r\partial_r\theta_h)] = 0 \tag{27}$$

Where,  $\theta_h$  and  $\sigma_h$  are the homotopy corresponding to the variables  $\theta$  and  $\sigma$ , and are expressed as,

$$\theta_h(r, q) = \theta_0 + q\theta_1 + q^2\theta_2 + q^3\theta_3 + \dots \tag{28}$$

and

$$\sigma_h(r, q) = \sigma_0 + q\sigma_1 + q^2\sigma_2 + q^3\sigma_3 + \dots \tag{29}$$

Where,  $q$  is a embedding parameter lying between  $0 \leq q \leq 1$ .  $\theta_0$  and  $\sigma_0$  are the solutions of the corresponding linear operators satisfying the boundary conditions as shown in the equation (21). We understand that the solution relies on  $q$ , and as the value of the embedding parameter changes from zero to one, the solutions of the variables  $\theta$  and  $\sigma$  are given by,

$$\theta = \lim_{q \rightarrow 1} \theta_h(r, q) = \theta_0 + \theta_1 + \theta_2 + \theta_3 + \dots \tag{30}$$

and

$$\sigma = \lim_{q \rightarrow 1} \sigma_h(r, q) = \sigma_0 + \sigma_1 + \sigma_2 + \sigma_3 + \dots \tag{31}$$

Substituting the equations (28) and (29) into the equations (26) and (27) and equating the coefficients of various powers of  $q$ , we get various order of deformations such as,

**Zerth-order deformation**

$$1/r \partial_r (r \partial_r \theta_0) = 0 \tag{32}$$

$$1/r \partial_r (r \partial_r \sigma_0) = 0 \tag{33}$$

corresponding boundary conditions for the outer and inner wall are,

$$\theta_0 = 1, \quad \sigma_0 = 1, \quad \text{at } r = r_c \tag{34}$$

$$\theta_0 = 0, \quad \sigma_0 = 0, \quad \text{at } r = R_1(z) \forall z \tag{35}$$

Initial guesses with respect to the linear operator are obtained from (32) - (35) as,

$$\theta_0 = \log (R_1(z)/r) / \log (R_1(z)/r_c) \tag{36}$$

$$\sigma_0 = \log (R_1(z)/r) / \log (R_1(z)/r_c) \tag{37}$$

Similarly higher order deformations  $\theta_1, \sigma_1, \theta_2, \sigma_2, \theta_3, \sigma_3, \dots$  could be computed.

In order to seek the solution for the axial velocity by using HPM, we have to incorporate the obtained temperature and concentration results. The corresponding PDE of the velocity profile having linear operator and non-linear operator is given below,

$$\underbrace{\left( \frac{\partial^2 v}{\partial r^2} + \frac{1}{r} \frac{\partial v}{\partial r} \right)}_L - \underbrace{\frac{\mu_f}{\mu_{nf}} \frac{\partial p}{\partial z}}_f - \underbrace{\frac{\eta_{nf} \mu_f}{\mu_{nf} \eta_f} \frac{1}{\beta^2} \Psi_r(v) + \frac{(\rho\gamma)_{nf} \mu_f}{(\rho\gamma)_f \mu_{nf}} (\theta Gr + \sigma Br)}_N = 0 \tag{38}$$

Here  $\Psi_r$  is described as  $\partial_{rr} + 1/r \partial_r$  and  $\partial_{rrrr} + 2/r \partial_{rrr} - 1/r^2 \partial_{rr} + 1/r^3 \partial_r$ . The boundary conditions (17) to (20) are used to solve the above equation.

The homotopy for the velocity variable is given below as,

$$v_h(r, q) = v_0 + q v_1 + q^2 v_2 + q^3 v_3 + \dots \tag{39}$$

Where  $v_0$  is the solution of the linear operator with significant conditions given at boundary. This is considered as initial guess for the above constructed homotopy. As embedding parameter moves from zero to one, axial velocity solution changes from  $v_0$  to  $v$ . Thus,

$$v = \lim_{q \rightarrow 1} v_h(r, q) = v_0 + v_1 + v_2 + v_3 + \dots \tag{40}$$

As done in case temperature and concentration we compare the coefficients of various powers of the embedding parameter  $q$  to get the various orders of deformations. The details are as given below.

**Zeroth order deformation**

$$1/r \partial_r(r \partial_r v_0) = 0 \tag{41}$$

with significant conditions at boundary are

$$v_0 = 0 \text{ at } r = r_c \text{ where } 0 \leq z \leq z_3 \tag{42}$$

For outer artery wall,

$$v_0 = u_2 \text{ at } r = R_1(z) \text{ where } d \leq z \leq d + L_0 \tag{43}$$

$$v_0 = u_1 \text{ at } r = R_1(z) \tag{44}$$

where  $0 \leq z \leq d$  and  $d + L_0 \leq z \leq z_{max}$

For inner artery wall,

$$v_0 = u_3 \text{ at } r = R_2(z) \text{ where } z_3 \leq z \leq z_{max} \tag{45}$$

Linear operator solution with the appropriate boundary conditions (42) - (45) is obtained as,

$$v_0 = \frac{u_2 \left( \log(r/r_c) \right)}{\left( \log(R_1(z)/r_c) \right)} \text{ Stenotic region} \tag{46}$$

$$v_0 = \frac{u_1 \left( \log(r/r_c) \right)}{\left( \log(R_1(z)/r_c) \right)} \text{ Non-stenotic region} \tag{47}$$

$$v_0 = \frac{u_3 \left( \log(r/R_2) \right)}{\left( \log(R_1(z))/R_2(z) \right)} \text{ Bifurcated region} \tag{48}$$

Similarly,  $v_1, v_2, v_3, \dots$  can be calculated. Through these obtained values, flow hemodynamics are determined. The computed values are used to evaluate the pressure gradient, volumetric flow rate. Further, the resistance to the flow and the wall shear stress is also computed.

**3.2 Hemodynamics flow parameters**

In this article, authors understood the hemodynamics of blood flow through a bifurcated stenotic artery. Flow dynamics of blood is altered due to the presence of obstruction in parent artery and bifurcation of the artery. These flow characteristics are defined as,

**Pressure Drop:** In circulatory system, pressure drop is occurring due to the action of heart pumping. From (14) the pressure drop can be calculated as,

$$\Delta P = \int_0^L \left[ \frac{\mu_{nf}}{\mu_f} \left( \partial_{rr} v + 1/r \partial_r v \right) - \frac{\eta_{nf}}{\eta_f} \frac{1}{\beta^2} \left( \partial_{rrrr} v + 2/r \partial_{rrr} v - 1/r^2 \partial_{rr} v + 1/r^3 \partial_r v \right) + \frac{(\rho\gamma)_{nf}}{(\rho\gamma)_f} (\theta Gr + \sigma Br) \right] dz \tag{49}$$

**WSS:** In the study of hemodynamics of bio-fluids, particularly for the cardiovascular diseases, the wall shear stress plays a vital role. Wall shear stress is expressed as the magnitude of the force that the blood exerts on the vessel walls and the force exerted by the endothelial cells to

the blood. The mathematical expression of WSS is given as,

$$\tau_{rz} = \underbrace{\mu_{nf} \frac{\partial v}{\partial r}}_{\tau_{rz}^S} + \frac{1}{4} \underbrace{\left[ \frac{\eta_{nf}}{r^2} \frac{\partial v}{\partial r} - \frac{\eta_{nf}}{r} \frac{\partial^2 v}{\partial r^2} - \eta_{nf} \frac{\partial^3 v}{\partial r^3} \right]}_{\tau_{rz}^A} \tag{50}$$

where,  $\tau_{rz}^S$  and  $\tau_{rz}^A$  represent the symmetrical and asymmetrical part of the stress tensor. After incorporating the non-dimensional parameters to the equation (50) we get,

$$\tau_{rz} = \underbrace{\mu_{nf} \frac{\partial v}{\partial r}}_{\tau_{rz}^S} + \frac{1}{4\beta^2} \frac{\mu_f}{\eta_f} \underbrace{\left[ \frac{\eta_{nf}}{r^2} \frac{\partial v}{\partial r} - \frac{\eta_{nf}}{r} \frac{\partial^2 v}{\partial r^2} - \eta_{nf} \frac{\partial^3 v}{\partial r^3} \right]}_{\tau_{rz}^A} \tag{51}$$

### §4 Results and Discussions

In this study, authors theoretically analyzed the hemodynamics of nanofluid flow through a catheterized bifurcated stenotic artery, which is driven by constant pressure gradient, and the resultant mathematical model is solved by using HPM. The results were obtained by incorporating the geometrical and non-dimensional parameters given as,  $a = 5, d = 10, L_0 = 5, \beta = \pi/10, \epsilon = 0.55a, r_2 = 0.51a, q = 0.15, z_1 = 20, u_1 = 0.5, u_2 = 0.25, u_3 = 0.75, N_b = 1, N_t = 0.2, Gr = 0.1, Br = 0.2, r_c = 0.01$ . For the validation of the method, we compared the tem-

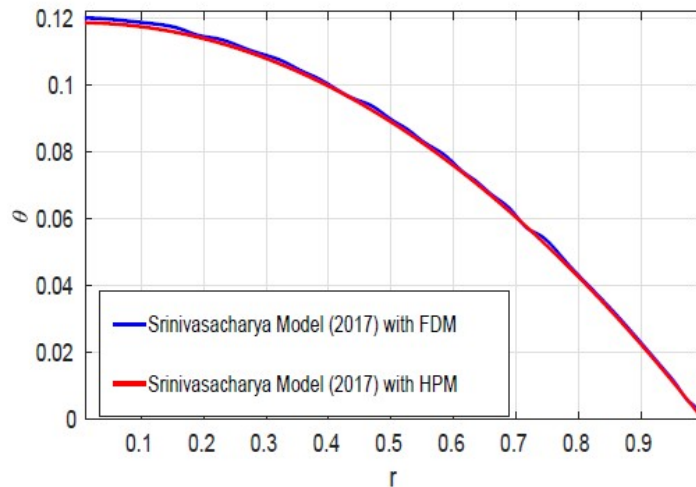


Figure 2. Comparison of temperature values computed from FDM of [14] and HPM (present method).

perature values of Srinivasacharya et al. [14] to the bifurcated stenotic model for  $Cu$ -water nanofluid at  $\Phi = 0.3$  in the parent artery as shown in Fig. 2. Wherein, the model of [14] has been used to obtained the results for temperature using HPM and same were compared with the finite difference method (FDM) numerical result of temperature. From the same figure, it is observed that the error is very less. Here, it was found that both the results are in good agreement. Hence use of HPM produces valid results for problems of this nature. Temperature

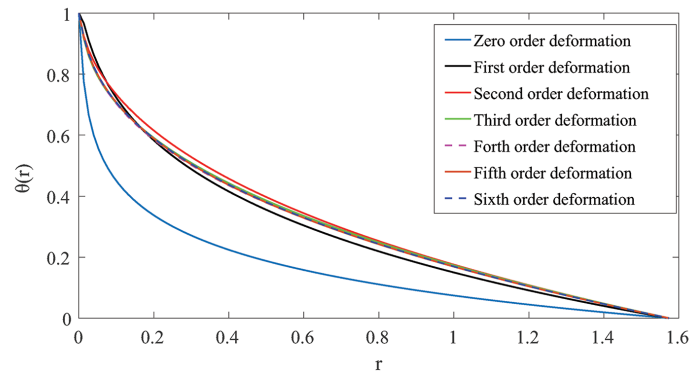


Figure 3. Temperature variation across radial direction  $r$  for various order of deformation.

values for various order of deformations is depicted in Fig. 3. From this figure, we observed that there is no variation from the fifth order deformation onwards, which speaks about the convergence of the method. Variations of axial velocities and wall shear stress are computed at the location  $z = 12.5$ , which is the location of maximum extrema, for various nano-fluids as shown in Figs. 4 and 5. In couple stress fluid, the axial velocity for  $Ag$ - NPs is comparatively higher than that of other NPs, while WSS distribution is least for  $Ag$ - NPs. Low shear stress allows the deposition of the cholesterol on the surface of the lumen, which initiates the development of atheroma. Hence, consideration of  $Ag$ - NPs for the treatment of chronic disease is not suitable. Accordingly, it appears that  $TiO_2$ - NPs are a good choice for analysing the flow dynamics. Further,  $TiO_2$ - NPs being ceramic in nature dissolve into the human body and also have several biomedical applications as mentioned in [44]. Hence,  $TiO_2$ - NPs are used for getting the subsequent results.

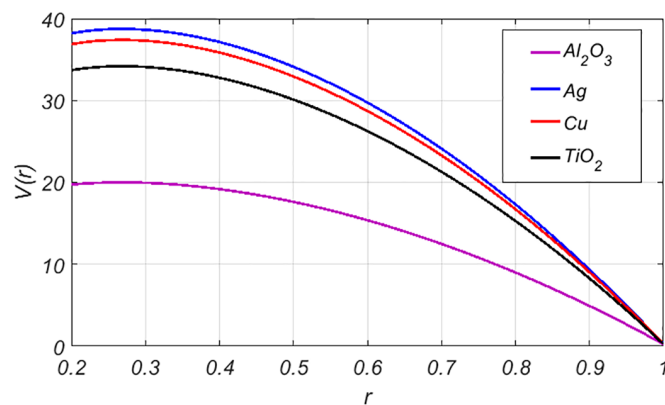


Figure 4. Comparison of axial velocities for different nanofluids in  $r$ - direction.

In the parent arterial wall, the axial velocity distribution is observed at different locations of the outer wall as shown in Fig. 6. Axial velocity is least at  $z = 12.5$  which corresponds to

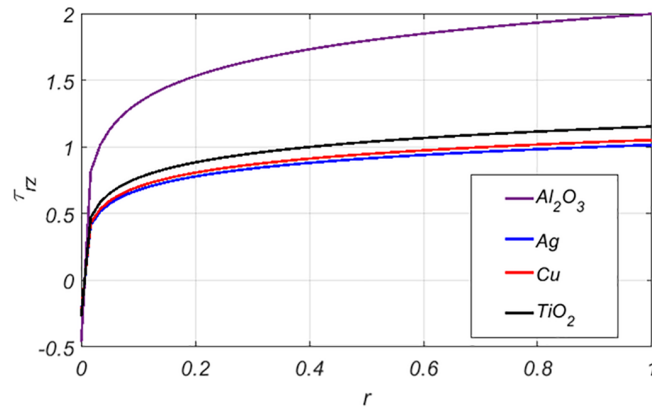


Figure 5. Comparison of WSS values for different nanofluids in  $r$ - direction.

the maximum height of stenosis. It is also observed that the axial velocity is more in the post-stenotic region than that in the pre-stenotic region. Volume fraction dependency of NPs on the blood is understood from Fig. 7. NPs enhance the thermal conductivity of the base fluid, which significantly depends on the volume fraction of the NPs, which is observed from the Figs. 6 and 7, that the axial velocity is less for the case where non-Newtonian fluid, while there is a rise in the velocity in case of increase of volume fraction of NPs. When volume fraction increases to  $\Phi = 2\%$  there is a sudden rise in the velocity due to the Brownian and thermophoretic parameters. It is also observed that for  $\Phi = 2\%$  and  $\Phi = 4\%$ , there is no variation in velocity profiles, hence,  $\Phi = 2\%$  has been considered in this study. Comparison of axial velocity profiles and wall

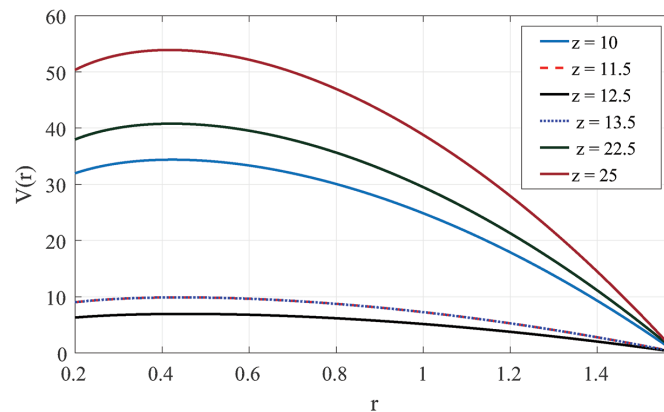


Figure 6. Variation of Axial velocity along radial direction  $r$  for various values of  $z$ .

shear stress for the fluid considered and Newtonian nanofluid are understood from Figs. 8 and 9. Here, even though the axial velocity is less in case of couple stress nanofluid, it is worth observing that WSS is more in non-Newtonian case. Therefore, understanding of blood flow dynamics using non-Newtonian structure is very crucial for conducting clinical procedures.

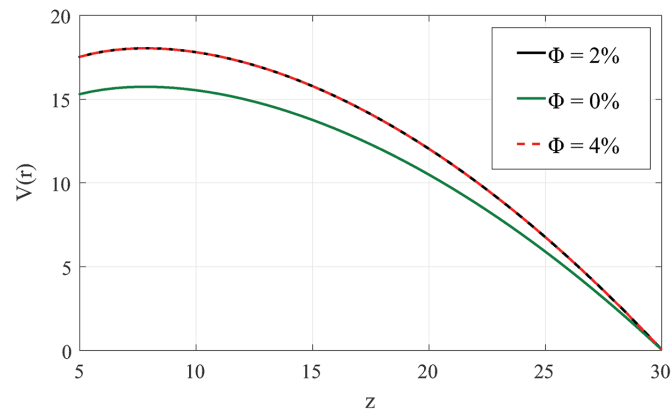


Figure 7. Axial velocity for various NPs for different values of  $\Phi$ .

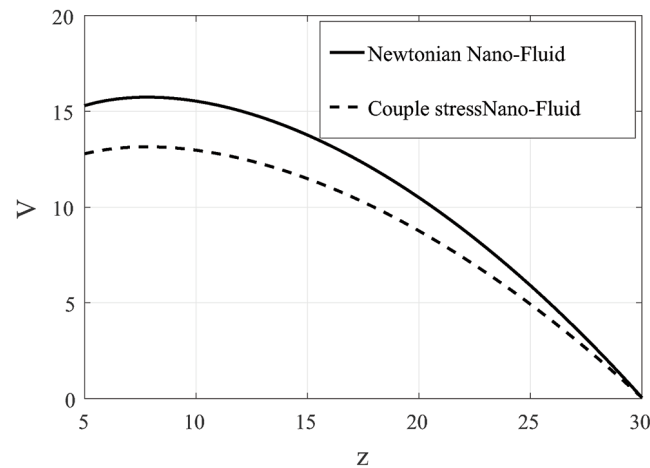


Figure 8. Comparison of axial velocities for Newtonian and non-Newtonian nanofluid.

Temperature and concentration distribution from catheter surface to the outer wall of a bifurcated artery, which is having mild stenosis is shown in Fig.10. Due to the presence of temperature sensitive NPs on the catheter, we observed higher temperature nearer to the catheter wall than at the arterial wall. It is realized that the temperature approaches to zero at the arterial wall justifying the boundary conditions considered. The rate of dispersion in temperature is decreasing from the catheter surface to the arterial wall. The fact that the dispersion rate is more at high temperature region is also observed from the left panel of Fig.10. Further, we have observed the least dispersion in the post-stenotic region. Hence, the dispersion is maximum in the stenotic region as desired, that being the region of interest. In similar lines, from the right panel of Fig.10 it is noticed that higher the concentration variation leads to the high concentration dispersion. In the axial direction, the drug diffusion is more at the extrema of the stenosis, which is prime for the faster delivery of the drug to the targeted region. In similar

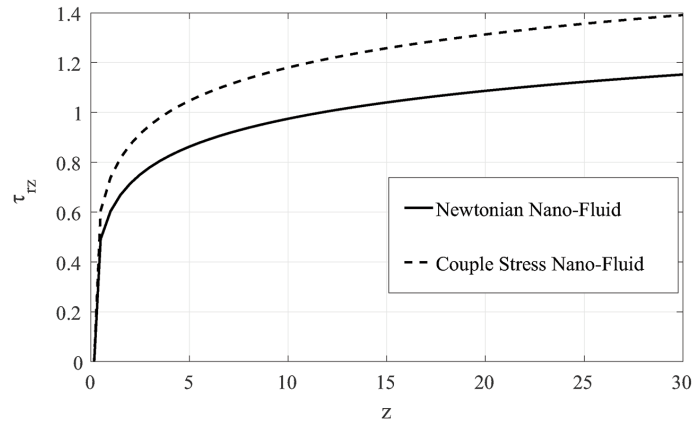


Figure 9. Comparison of WSS values for Newtonian and non-Newtonian nanofluid.

lines, temperature and concentration profiles are analyzed for the inner wall of a bifurcated artery across the axial and radial directions, and is depicted in Fig.10. It is observed that the

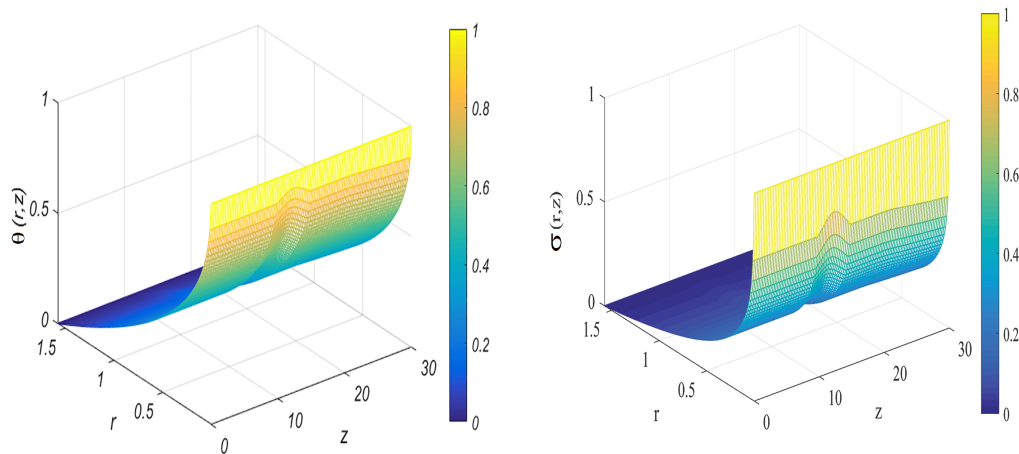


Figure 10. Distribution along  $z$ - and  $r$ - directions at the outer wall(Left:Temperature values, Right: Concentration values).

temperature and concentration distribution are more near to the apex of the flow division due to the disturbance of flow. From the Fig.11, we can clearly see a small vortex structures in the considered domain, hence more temperature and concentration dispersion is observed near to the flow division. Far away from the apex the temperature and concentration dispersion do not have significant influence on the daughter arteries, which is good indeed. This understanding could probably provide a new approach towards a sustainable and controlled drug delivery to the targeted organs of the human body.

Authors have analysed the axial velocity profiles for outer arterial wall as well as for the

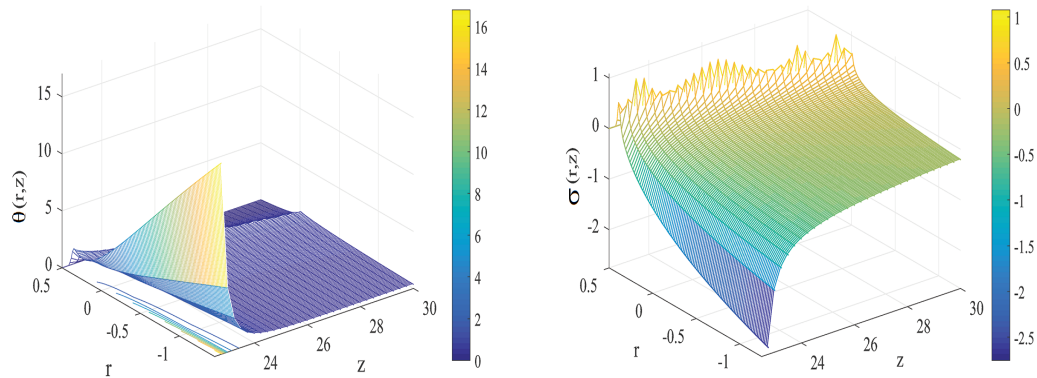


Figure 11. Distribution along  $z$ - and  $r$ - directions at the inner wall (Left: Temperature values, Right: Concentration values).

inner arterial wall of a bifurcated artery and the results as given in Fig. 12. In the parent artery wall, the axial velocity distribution is observed at different locations of the outer wall as shown in the left panel of Fig.12. Corresponding to the maximum height of the stenosis the axial velocity is very less due to the very small annular region between the catheter surface and the outer arterial wall. However, axial velocity is more in the post-stenotic region of the stenosis than that of pre-stenotic region of the stenosis. Axial velocity is found to be comparatively more at the outer wall of the daughter bifurcated artery than that of outer wall of the parent artery. The variation in the axial velocity is more at the catheter surface than at the arterial surface. In the case of outer wall, axial velocity profile is less at the extrema of stenosis than at pre and post stenotic regions of the parent artery, while for the outer wall of the daughter artery, velocity is moderately less nearer to the apex than at the other regions. Such flow behavior occurs due to the increasing occlusion and reduced annular region for the flow of blood. Similarly, velocity profile for the inner arterial wall can be seen from the right panel of Fig.12. At the division walls of the bifurcations site, the boundary layers are relatively thin with the maximum axial velocity outside the boundary layer. As the blood enters the daughter arteries with a finite radius of curvature, the faster moving fluid is observed at the flow divider due to secondary flow development. Corners of outer wall being sharp, a flow separation is observed along the outer wall of the bifurcation.

WSS distribution at the outer arterial wall is depicted in Fig.13. WSS has considerable clinical relevance because it provides information about the magnitude of the force that the blood exerts on the vessel wall as well as the force exerted by the fluid. Low WSS is related to the atherosclerosis, and also low WSS impairs the mass transport between blood and the vessel wall. From Fig.13, it is noticed that WSS is least in the stenotic region and it slightly increases from the bifurcation point when compared to that of non-stenotic region.ear to the region of the flow division i.e., in the daughter artery. This is because of the presence of circulatory flow which results in less velocity gradient and hence low WSS. Atherosclerosis is correlated with the pressure and low WSS into the human aorta. As the blood is forced to turn around the curve pressure will increase on outer wall and correspondingly decrease at the curvature.

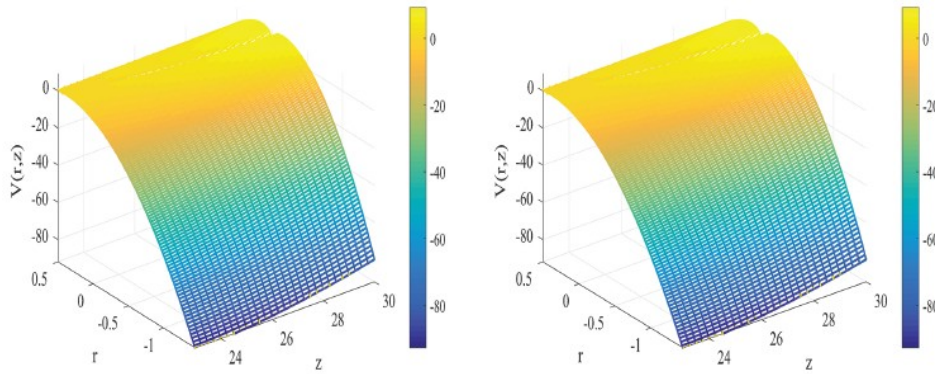


Figure 12. Axial velocity distribution along  $z$ - and  $r$ - direction (Left:At the outer wall Right: At the inner wall).

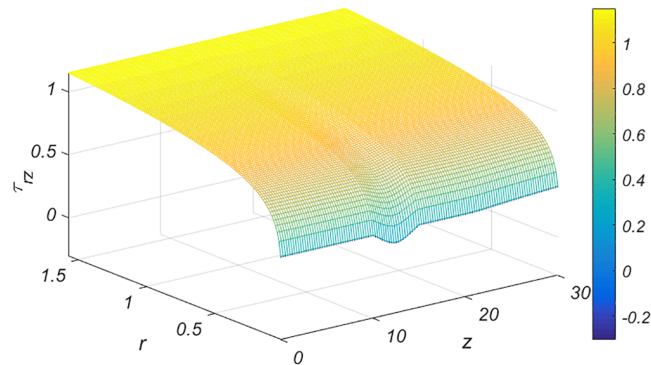


Figure 13. WSS distribution along  $z$ - and  $r$ - direction at the outer wall.

Hence, these phenomena allow endothelium deposition into the lumen, starting of the disease process. in this study we have stenotic region from  $z = 10$  to  $z = 15$  and location  $z = 12.5$  is the location of extremes.

## §5 Conclusion

This theoretical study have immense important role in order to understand the physiology of surgical and intervention treatment. We have discussed the flow dynamics related to the realistic geometry of interest. Some typical observations are as given below,

1. It is observed that results are converging from the fourth deformation onwards for the parameter of interest. One particular case of temperature in depicted in one of the figures.
2.  $TiO_2$ - NPs have been chosen for the analysis due to their moderately high velocity profiles

and relatively high wall shear stress.

3. WSS is more for couple stress nanofluid than that of Newtonian nanofluid while results are exactly reversed for velocity profiles.
4. It is observed that the volume fraction enhances the temperature and concentration dispersion.
5. It is noticed that the rate of temperature and concentration dispersion is more at the constricted region than that at the outer arterial wall.
6. In case of inner arterial wall of a bifurcated artery, it is observed that apex has more temperature and concentration distribution both in axial and radial direction.
7. Flow parameter are in good deed in order to extrapolate these to the clinical investigation.

This theoretical mathematical model and its related observations represents a prototype to the physicians and research scientist in pathology, biomedical and in pharmaceutical industry.

## References

- [1] *World health statistics 2018: monitoring health for the sdgs, sustainable development goals*, World Health Organization, et al, 2018.
- [2] A Arab, A Alfi. *An adaptive gradient descent-based local search in memetic algorithm applied to optimal controller design*, Inform Sciences, 2015, 299: 117-142.
- [3] D F Young, F Y Tsai. *Flow characteristics in models of arterial stenoses –I. Steady flow*, J Biomech, 1973, 6(4): 395-402.
- [4] D F Young, F Y Tsai. *Flow characteristics in models of arterial stenoses –II. Unsteady flow*, J Biomech, 1973, 6(5): 547-559.
- [5] T N D Ariman, M A Turk, N D Sylvester. *Applications of microcontinuum fluid mechanics*, Int J Eng Sci, 1974, 12(4): 273-293.
- [6] G Bugliarello, J Sevilla. *Velocity distribution and other characteristics of steady and pulsatile blood flow in fine glass tubes*, Biorheology, 1970, 7(2): 85-107.
- [7] V K Stokes. *Couple stresses in fluids*, Phys Fluids, 1966, 9(9): 1709-1715.
- [8] K B Chandran. *Flow dynamics in the human aorta*, J Biomech Eng, 1993, 115(4B): 611-616.
- [9] S Chakravarty, P K Mandal. *An analysis of pulsatile flow in a model aortic bifurcation*, Int J Eng Sci, 1997, 35(4): 409-422.
- [10] M C Truss, C G Stief, U Jonas. *Werner forssmann: surgeon, urologist, and nobel prize winner*, World J Urol, 1999, 17(3): 184-186.
- [11] A B M Hasan, D K Das. *Numerical simulation of sinusoidal fluctuated pulsatile laminar flow through stenotic artery*, J Appl Fluid Mech, 2008, 1(2): 25-35.
- [12] J V R Reddy, D Srikanth, SVSSNVG Krishna Murthy. *Mathematical modelling of pulsatile flow of blood through catheterized unsymmetric stenosed artery-effects of tapering angle and slip velocity*, Eur J Mech B Fluids, 2014, 48: 236-244.

- [13] D Srinivasacharya, G M Rao. *Pulsatile flow of couple stress fluid through a bifurcated artery*, Ain Shams Eng J, 2018, 9(4): 883-893.
- [14] A A Farooq, D Tripathi, T Elnaqeeb. *On the propulsion of micropolar fluid inside a channel due to ciliary induced metachronal wave*, Appl Math Comput, 2019, 347: 225-235.
- [15] T Elnaqeeb. *Modeling of Au(NPs)-blood flow through a catheterized multiple stenosed artery under radial magnetic field*, Eur Phys J Special Topics, 2019, 228: 2695-2712.
- [16] D Srinivasacharya, G M Rao. *Modeling of blood flow through a bifurcated artery using nanofluid*, BioNanoScience, 2017, 7(3): 464-474.
- [17] Elnaqeeb, Thanaa, Nehad Ali Shah, Khaled S Mekheimer. *Hemodynamic characteristics of gold nanoparticle blood flow through a tapered stenosed vessel with variable nanofluid viscosity*, BioNanoScience, 2019, 9: 245-255.
- [18] Mekheimer, Khaled S, Mohamed S Mohamed, Thanaa Elnaqeeb. *Metallic nanoparticles influence on blood flow through a stenotic artery*, International Journal of Pure and Applied Mathematics, 2016, 107(1): 201.
- [19] Mekheimer, et al. *Simultaneous effect of magnetic field and metallic nanoparticles on a micropolar fluid through an overlapping stenotic artery: Blood flow model*, Physics Essays, 2016, 29(2): 272-283.
- [20] M Hatami, D D Ganji. *Motion of a spherical particle in a fluid forced vortex by dqm and dtm*, Particuology, 2014, 16: 206-212.
- [21] Wenhui Tang, M Hatami, Jiandong Zhou, Dengwei Jing. *Natural convection heat transfer in a nanofluid-filled cavity with double sinusoidal wavy walls of various phase deviations*, International Journal of Heat and Mass Transfer, 2017, 115: 430-440.
- [22] O Pourmehran, M Rahimi-Gorji, M Hatami, S A R Sahebi, G Domairry. *Numerical optimization of microchannel heat sink (mchs) performance cooled by kkl based nanofluids in saturated porous medium*, Journal of the Taiwan Institute of Chemical Engineers, 2015, 55: 49-68.
- [23] M Hatami. *Nanoparticles migration around the heated cylinder during the rsm optimization of a wavy-wall enclosure*, Advanced Powder Technology, 2017, 28(3): 890-899.
- [24] M Sheikholeslami, M Hatami, D D Ganji. *Numerical investigation of nanofluid spraying on an inclined rotating disk for cooling process*, Journal of Molecular Liquids, 2015, 211: 577-583.
- [25] Jiandong Zhou, M Hatami, Dongxing Song, Dengwei Jing. *Design of microchannel heat sink with wavy channel and its time-efficient optimization with combined rsm and fvm methods*, International Journal of Heat and Mass Transfer, 2016, 103: 715-724.
- [26] M Hatami, Dongxing Song, Dengwei Jing. *Optimization of a circular-wavy cavity filled by nanofluid under the natural convection heat transfer condition*, International Journal of Heat and Mass Transfer, 2016, 98: 758-767.
- [27] M Hatami, J Zhou, J Geng, D Song, D Jing. *Optimization of a lid-driven t-shaped porous cavity to improve the nanofluids mixed convection heat transfer*, Journal of Molecular Liquids, 2017, 231: 620-631.
- [28] G L Liu. *New research directions in singular perturbation theory: artificial parameter approach and inverse-perturbation technique*, In Conference of 7th modern mathematics and mechanics, 1997, 47-53.
- [29] Shi-Jun Liao. *An approximate solution technique not depending on small parameters: a special example*, International Journal of Non-Linear Mechanics, 1995, 30(3): 371-380.

- [30] Ji-Huan He. *Variational iteration method for autonomous ordinary differential systems*, Applied Mathematics and Computation, 2000, 114(2-3): 115-123.
- [31] Ji-Huan He. *Homotopy perturbation technique*, Computer methods in applied mechanics and engineering, 1999, 178(3-4): 257-262.
- [32] KM Surabhi, J V Ramana Reddy, D Srikanth. *Impact of temperature and concentration dispersion on the physiology of blood nanofluid: links to atherosclerosis*, Sadhana, 2018, 43(12): 210.
- [33] J V Ramana Reddy, D Srikanth, Samir K Das. *Modelling and simulation of temperature and concentration dispersion in a couple stress nanofluid flow through stenotic tapered arteries*, The European Physical Journal Plus, 2017, 132(8): 365.
- [34] Robin Fahraeus, Torsten Lindqvist. *The viscosity of the blood in narrow capillary tubes*, American Journal of Physiology-Legacy Content, 1931, 96(3): 562-568.
- [35] G K Batchelor. *The effect of brownian motion on the bulk stress in a suspension of spherical particles*, Journal of fluid mechanics, 1977, 83(1): 97-117.
- [36] M Hatami, J Hatami, Davood Domiri Ganji. *Computer simulation of mhd blood conveying gold nanoparticles as a third grade non-newtonian nanofluid in a hollow porous vessel*, Computer methods and programs in biomedicine, 2014, 113(2): 632-641.
- [37] Bock Choon Pak, Young I Cho. *Hydrodynamic and heat transfer study of dispersed fluids with submicron metallic oxide particles*, Experimental Heat Transfer an International Journal, 1998, 11(2): 151-170.
- [38] L Godson, B Raja, D Mohan Lal, S Wongwises. *Experimental investigation on the thermal conductivity and viscosity of silver-deionized water nanofluid*, Experimental Heat Transfer, 2010, 23(4): 317-332.
- [39] H C Brinkman. *The viscosity of concentrated suspensions and solutions*, The Journal of Chemical Physics, 1952, 20(4): 571-571.
- [40] R L Hamilton, O K Crosser. *Thermal conductivity of heterogeneous two-component systems*, Industrial & Engineering chemistry fundamentals, 1962, 1(3): 187-191.
- [41] Jacopo Buongiorno. *Convective transport in nanofluids*, Journal of heat transfer, 2006, 128(3): 240-250.
- [42] P Chaturani, D Biswas. *A comparative study of poiseuille flow of a polar fluid under various boundary conditions with applications to blood flow*, Rheologica acta, 1984, 23(4): 435-445.
- [43] P Brunn. *The velocity slip of polar fluids*, Rheologica Acta, 1975, 14(12): 1039-1054.
- [44] Zi Fei Yin, Long Wu, Hua Gui Yang, Yong Hua Su. *Recent progress in biomedical applications of titanium dioxide*, Physical chemistry chemical physics, 2013, 15(14): 4844-4858.

<sup>1</sup>Department of Applied Mathematics, Defence Institute of Advanced Technology (Deemed University), Girinagar Pune 411025, India.

Email: sri\_dasari1977@yahoo.co.in

<sup>2</sup>Department of Mathematics, National Institute of Technology, Warangal 506004, India.